Received: 20 November 2022 | Revised: 20 December 2022 | Accepted: 27 December 2022

DOI: 10.1002/agt2.314

Aggregate WILEY Open Access

RESEARCH ARTICLE

Phase separation-induced nanoprecipitation for making polymer nanoparticles with high drug loading

Guangze Yang[1,2] | **Yun Liu**[1,2] | **Song Jin**[1,2] | **Yue Hui**[1] | **Xing Wang**[1,2] | **Letao Xu**[1,2] | **Dong Chen**[3,4] | **David Weitz**[5,6] | **Chun-Xia Zhao**[1,2]

[1]School of Chemical Engineering, Faculty of Sciences, Engineering and Technology, The University of Adelaide, Adelaide, South Australia, Australia

[2]Australian Institute for Bioengineering and Nanotechnology, The University of Queensland, Brisbane, Queensland, Australia

[3]Department of Medical Oncology, The First Affiliated Hospital, School of Medicine, Zhejiang University, Hangzhou, Zhejiang, China

[4]College of Energy Engineering and State Key Laboratory of Fluid Power and Mechatronic Systems, Zhejiang University, Hangzhou, Zhejiang, China

[5]John A. Paulson School of Engineering and Applied Sciences, Harvard University, Cambridge, Massachusetts, USA

[6]Department of Physics, Harvard University, Cambridge, Massachusetts, USA

Correspondence
Chun-Xia Zhao, School of Chemical Engineering, Faculty of Sciences, Engineering and Technology, The University of Adelaide, Adelaide, SA 5005, Australia.
Email: chunxia.zhao@adelaide.edu.au

Funding information
Australian Research Council, Grant/Award Number: DP200101238; National Health and Medical Research Council projects of Australia, Grant/Award Number: APP2008698

Abstract

Increasing drug loading remains a critical challenge in the development and translation of nanomedicine. High drug-loading nanoparticles have demonstrated unique advantages such as less carrier material used, better-controlled drug release, and improved efficacy and safety. Herein, we report a simple and efficient salt concentration screening method for making polymer nanoparticles with exceptionally high drug loading (up to 66.5 wt%) based on phase separation-induced nanoprecipitation. Upon addition of salt, phase separation occurs in a miscible solvent-water solution delaying the precipitation time of drugs and polymers to different extents, facilitating their co-precipitation thus the formation of high drug-loading nanoparticles with high encapsulation efficiency (>90%) and excellent stability (>1 month). This technology is versatile and easy to be adapted to various hydrophobic drugs, different polymers, and solvents. This salt-induced nanoprecipitation strategy offers a novel approach to fabricating polymer nanoparticles with tunable drug loading, and opens great potentials for future nanomedicines.

KEYWORDS

drug loading, liquid-liquid phase separation, nanoparticles, nanoprecipitation, salt

1 | INTRODUCTION

Nanoprecipitation is a simple but widely used method for preparing drug-loaded polymer nanoparticles.[1–3] Typically, an organic solvent containing a polymer and a drug is added to an antisolvent (e.g. water or a buffer solution) under mixing to form drug-loaded polymer nanoparticles.[1,4,5] Drug loading (w_{drug} / $w_{drug + polymer}$) of the polymer nanoparticles using this method is generally low (<10 wt%), mainly due to the significant difference in the precipitation time of the drug and the polymer, so the polymer often precipitates before the drug, resulting in empty polymer nanoparticles with drug aggregates or crystals.[4,6,7] Compared to low drug-loading nanoparticles, high drug-loading nanoparticles have demonstrated several unique advantages such as less carrier material used, better-controlled drug release, and improved efficacy and safety.[8,9] From our previous studies, high drug-loading nanoparticles could have better-controlled release compared to the low drug-loading nanoparticles as the drug release can be controlled by either tuning the drug loading thus controlling the dissolution time of the drug core, or adjusting the polymer compositions of the shell.[10,11] Therefore, it is of great interest to develop new strategies to increase drug loading. One approach is to use fast mixing to co-precipitate the drug and polymer, for example, microfluidic flow-focusing or flash nanoprecipitation.[12–14] Alternatively, sequential nanoprecipitation is able to control the precipitation times of the drug and polymer using solvent mixtures, so the drug precipitates first followed by the polymer thus

Guangze Yang and Yun Liu contributed equally.

forming drug-core polymer-shell with high drug loading.[11] On the other hand, salt-induced precipitation offers a new strategy for controlling precipitation time.

Salting out has been widely used for protein purification.[15,16] It relies on the principle that proteins become less soluble in solutions of high salt concentrations due to the shielding effect of salt ions.[17] As the solubility of different proteins is different at the same salt concentration, proteins can be separated using this salting out process.[18] Similarly, polymers can be precipitated out using the salting-out method.[19] A liquid-liquid two-phase system can be obtained by adding a viscous gel containing saturated magnesium chloride/acetate and poly(vinyl alcohol) to acetone containing poly(DL-lactic acid) under mechanical stirring, forming an oil-in-water emulsion.[20] Polymer nanoparticles can be subsequently generated by adding more water to the emulsion.

Inspired by this well-known salting-out process, we attempt to use salt-induced precipitation to create polymer nanoparticles with high drug loading. Theoretically, the precipitation time of a polymer and a drug could be tuned by varying salt concentrations. At the right salt concentration, they could co-precipitate or precipitate sequentially. Based on this hypothesis, we designed a simple salt-concentration screening method to obtain polymer nanoparticles with tunable drug loading up to 66.5 wt%. To fundamentally understand salt-induced nanoprecipitation, we systematically studied salt-induced liquid-liquid separation and its associated nanoprecipitation. This new salt-induced nanoprecipitation approach offers a simple and versatile method for preparing different nanoparticles with tunable drug loadings.

2 | EXPERIMENTAL SECTION

2.1 | Materials

Docetaxel was purchased from Shanghai Titan Scientific Co., Ltd. (Shanghai, China). Poly(lactide-co-glycolide)-b-poly(ethylene glycol) (PLGA-PEG) of $PLGA_{10k}$-PEG_{5k} and $PLGA_{55k}$-PEG_{5k}, poly(lactic acid)-PEG (PLA_{9k}-PEG_{3k}), and poly(caprolactone) (PCL_{20k}-PEG_{5k}) were purchased from PolySciTech (Akina, West Lafayette, IN). Dimethylformamide (DMF) and curcumin were purchased from Merck (Bayswater, Australia). Phosphate buffered saline (PBS) was purchased from Thermo Fisher Scientific (Scoresby, Australia). FITC-$Dextran_{40k}$, tetramethylindocarbocyanine perchlorate (DiI), ibuprofen, and dimethyl sulfoxide (DMSO) were purchased from Sigma Aldrich Pty Ltd (North Ryde BC, Australia). Ketamine was purchased from Novachem Pty Ltd (Heidelberg West, Australia). Shellac was purchased from Sigma-Aldrich, Inc. (St. Louis, MO). Water having resistivity larger than 18.2 MΩ·cm was obtained from a Milli-Q system (Merck, Bayswater, Australia) equipped with a 0.22 μm filter.

2.2 | Salt screening method for making polymer nanoparticles with high drug loadings

To make 50 wt% docetaxel-loading $PLGA_{10k}$-PEG_{5k} nanoparticles, docetaxel and $PLGA_{10k}$-PEG_{5k} were dissolved in 50 μL DMF at a concentration of 5 g/L. The pH of all different concentrations (1× to 20×) of PBS was adjusted to 7.4. 200 μL PBS with different salt concentrations were added to the DMF and mixed for around three seconds in a dry and clean glass vial, followed by the addition of 750 μL water and mixed well. The nanoparticle suspension was then dialyzed against 1× PBS using a dialysis membrane having molecular weight cut-off (MWCO) of 100 kDa for 16 h at 4°C to remove solvent and balance salt concentration, followed by centrifugation at 100 g for 3 min and collection of the supernatant. Other drug- or dye- loaded nanoparticles were prepared using the same method. Another buffer system containing 25 mM HEPES and 0–9% NaCl at pH 7 was also employed to produce docetaxel-loaded $PLGA_{10k}$-PEG_{5k} nanoparticles with an initial 50% drug loading using the same method described above.

2.3 | Characterization of polymer nanoparticles with high drug loadings

The hydrodynamic size and polydispersity index (PDI) of the synthesized nanoparticles were determined using a Zetasizer Nano ZS (ATA Scientific, Taren Point, Australia). The morphology of nanoparticles was observed using a transmission electron microscope (TEM) (Hitachi Australia Pty. Ltd., North Ryde, Australia). Nanoparticles for TEM samples were dropped onto a copper TEM grid with a carbon film followed by negative staining using 1% uranyl acetate.

2.4 | Drug loading measurement

Drug-loaded nanoparticles were fabricated and dialyzed against water twice using a dialysis membrane having molecular weight cut-off (MWCO) of 100 kDa for 6 h to remove all solvents and salts, followed by centrifugation at 100 g for 3 min and collection of the supernatant. The supernatant was lyophilized for 72 h and then weighed its mass as *m*(*drug_loadedNP*). The lyophilized powder was dissolved in DMSO, and the drug concentration was analyzed by a reversed-phase high-performance liquid chromatography (RP-HPLC) (Shimadzu, Kyoto, Japan) equipped with a Jupiter C18 column (5 μm; 300 Å; 150 mm × 4.6 mm) (Phenomenex, Torrance, CA), to calculate the drug weight *m* (*drug*). The drug loading was calculated by using the following equation:

$$\text{Drugloading} = \frac{\text{m (drug)}}{\text{m (drug\_loadedNP)}} \quad (1)$$

2.5 | Encapsulation efficiency measurement

Drug-loaded nanoparticles were fabricated and then diluted by a factor of 5 using water. The quantity of the added drug was determined as *m* (*drug initially added*). The suspension was aged for 1 h, followed by low-speed centrifugation (100 g, 3 min) to remove drug aggregates. The supernatant was collected and lyophilized for 72 h. The lyophilized powder was dissolved by DMSO, and the drug concentration was analyzed by the RP-HPLC to calculate the drug weight *m* (*drug in NP*). The encapsulation efficiency was calculated

by using the following equation:

$$\text{Encapsulation efficiency} = \frac{\text{m (drug in NP)}}{\text{m (drug initially added)}} \quad (2)$$

2.6 | Nanoparticle stability test

The purified nanoparticles with high drug loading were incubated at 4°C. At the pre-set time points, an aliquot of the nanoparticle suspension was taken for hydrodynamic size and PDI measurement using DLS.

2.7 | Fluorescence labeling of salt-induced liquid-liquid phase separation

At different PBS/DMF volume ratios, FITC-Dextran$_{40k}$ was dissolved in 7× PBS with different concentrations (0.133 to 0.6 g/L). 40 to 600 μL 7× PBS containing FITC-Dextran$_{40k}$ was added to 200 μL DMF and mixed well to make PBS/DMF volume ratios of 0.2:1 to 3:1. The final FITC-Dextran$_{40k}$ concentration of all samples was kept the same as 0.1 g/L. 100 μL suspension was taken to be observed under a fluorescent microscope (Nikon, Tokyo, Japan) with an excitation of 470 nm. The excitation filter was 480/30 nm and the emission filter was 535/45 nm.

For the samples of different salt concentrations, FITC-Dextran$_{40k}$ was dissolved in different concentrations of PBS (1× to 15×) at a concentration of 0.2 g/L. 200 μL PBS containing FITC-Dextran$_{40k}$ with different salt concentrations was added to 200 μL DMF and mixed well. The final FITC-Dextran$_{40k}$ concentration of all samples was kept the same at 0.1 g/L. 100 μL suspension was taken to be observed under a fluorescent microscope (Nikon, Tokyo, Japan) with an excitation of 470 nm.

2.8 | Accumulative precipitation diagrams of drugs and polymers

200 μL DMF containing drugs (5 g/L) or polymers (5 g/L) were mixed with PBS with different volumes (step of 40 μL) and salt concentrations (1, 3, 5, and 7×) in a quartz cuvette, and the DCR of the mixture was measured. The DCR of the mixture of pure DMF and PBS was considered blank and subtracted. The product of DCR and the volume of the mixture was calculated to obtain the accumulative precipitation diagrams. The nanoprecipitation was considered to be completed when the product of DCR and the volume of the mixture stopped increasing. The increase of accumulative nanoprecipitation between each PBS addition to the solvent was plotted as the distributive nanoprecipitation diagrams, and the quantity of the entire accumulative nanoprecipitation was used as 100% for the distributive nanoprecipitation.

2.9 | Statistical analysis

Statistics were computed using GraphPad Prism 9. Standard unpaired two-tailed Student's t test was used to test for statistical significance between groups, with $P < 0.001$ denoted as ***. Values for P are included in the appropriate figure legend or the main text.

3 | RESULTS AND DISCUSSION

Traditional nanoprecipitation is to add a solvent solution containing a drug and a polymer to a large volume of an antisolvent (water or a buffer solution) with stirring. Instead, a reversed nanoprecipitation, that is, adding an antisolvent to a solvent solution, was used to slow down the precipitation of drug and polymer, thus allowing more time to form uniform nanoparticles.[11]

3.1 | Salt concentration screening

Basically, we made a series of solutions with different salt concentrations as the antisolvent. The commonly used phosphate buffered saline (PBS) is selected due to its buffering capability, high solubility, and a wide range of tunable salt concentrations.[21] 200 μL 1× to 10× PBS (Table S1, all pH adjusted to 7.4) was added to an organic solvent dimethylformamide (DMF) of 50 μL containing a model anti-cancer drug docetaxel and a U.S. Food and Drug Administration (FDA)-approved polymer poly(D,L-lactide-co-glycolide)-block-poly(ethylene glycol) (PLGA$_{10k}$-PEG$_{5k}$), followed by the addition of 750 μL water and dialysis in 1× PBS to remove DMF and reduce the salt concentration (Figure 1A,B). The additional dilution and dialysis are critical for limiting the solvent-related Ostwald ripening and salt-induced aggregation.[22–25] The mass concentrations of docetaxel and PLGA-PEG in the solvent were kept the same (5 g/L in DMF), so the initial theoretical drug loading was 50 wt%.

Interestingly, we observed quite different results among the samples that used different salt concentrations. Some salt concentrations produced clear nanoparticle suspension, whereas others generated obvious drug aggregates and precipitate out in the end. More specifically, 2, 3, 4, and 7× PBS result in the formation of small nanoparticles (<250 nm) with low polydispersity (PDI, <0.25), indicating the successful encapsulation of the drug in polymer nanoparticles (Figure 1C and Table S2), in other words, the successful formation of polymer nanoparticles with high drug loading and high drug encapsulation efficiency (close to the theoretical drug loading of 50% and nearly 100% encapsulation efficiency). However, other PBS concentrations produced apparent drug precipitates.

The significant effect of salt concentrations on the formation of drug-loaded nanoparticles may be attributed to the different solubilities thus different precipitating time of drugs and polymers under different salt concentrations. Under certain salt concentrations, a drug could precipitate before or co-precipitate with a polymer, instead of precipitating after the polymer, creating opportunities for effective encapsulation.

Notably, we also attempted the formation of drug-encapsulated polymer nanoparticles using these four salt concentrations and the traditional precipitation sequence, i.e., injecting the solvent into the antisolvent while stirring. However, big aggregates formed in the obtained suspensions

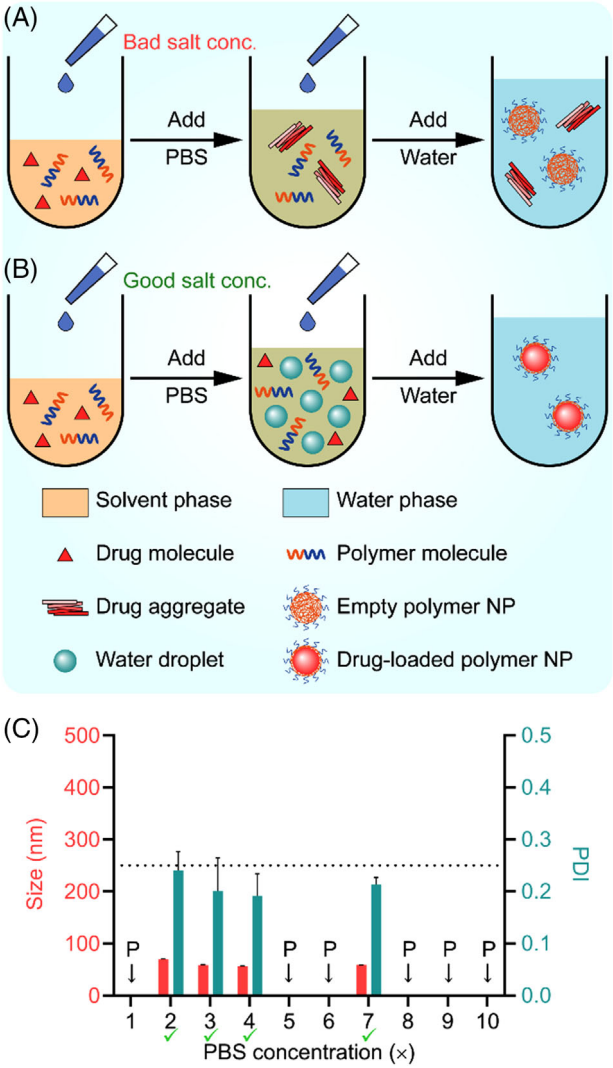

FIGURE 1 Schematic of the salt-concentration screening method. An antisolvent containing salts of different concentrations is added to a solvent solution containing a drug and a polymer. (A) For bad salt concentrations, the drug precipitates and forms aggregates. (B) For good salt concentrations, salts induce the formation of micron water droplets which delay the precipitation of the drug and the polymer resulting in their co-precipitation, thus forming nanoparticles with high drug loading. (C) The salt concentration screening result for 50 wt% docetaxel-loaded $PLGA_{10k}$-PEG_{5k} nanoparticles. Green ticks indicate good formulations.

within one hour, demonstrating that the reversed precipitation sequence is critical in this salt-concentration screening method. This novel screening method is rapid and simple for identifying good formulations with high drug loading. Moreover, it does not require specific devices.

3.2 | Effect of salt concentration on drug encapsulation

We further investigated two typical PBS concentrations, 1× and 7×, a commonly used salt concentration in traditional nanoprecipitation and the highest salt concentration of the four good candidates after our screening. Their solutions looked significantly different, with large quantities of white aggregates indicating unencapsulated docetaxel in 1× PBS but very clear suspension without any aggregates in 7× PBS (Figure 2A,B). Transmission electron microscopy (TEM) images further revealed their difference. Micron-sized drug crystals were observed in 1× PBS, by contrast, well-dispersed and uniform high drug-loading polymer nanoparticles with a size around 50 nm were detected in 7× PBS (Figure 2A,B and Figure S1). The TEM morphology of these two samples suggested that the drug precipitated after the polymer in 1× PBS formed drug aggregates. Nevertheless, 7× PBS seemed to allow the co-precipitation of the drug and the polymer thus forming polymer nanoparticles with high drug loading.[11]

Then, we compared the encapsulation efficiency of these two representative samples. As the drug precipitates (unencapsulated) can be easily separated from the drug-loaded nanoparticles (encapsulated) by low-speed centrifugation,[11] the encapsulation efficiency can be calculated based on the drug content remaining in the supernatant. Being consistent with the appearance of the suspension and TEM images, the encapsulation efficiency of the nanoparticles made using 1× PBS was much lower (46.7%) than that using 7× PBS (98.2%) (Figure 2C).

Good stability is very important for nanoparticles with high drug loading[26] which may have a high propensity towards aggregation during storage due to their overall high hydrophobic fractions. We examined the stability of all the four good formulations (2×, 3×, 4×, and 7× PBS) at 4°C (Figure 2D). Both the size and PDI of the four nanoparticle suspensions remained stable over 35 days, demonstrating their excellent stability (Tables S3 and S4). The long-term stability of the four nanoparticle suspensions suggested that the drug was well encapsulated inside the nanoparticles, instead of coating or adsorbing on the nanoparticle surfaces, which could lead to a quick release thus the formation of drug aggregates and significant changes of size and PDI.[27] We kept monitoring these four formulations till 56 days, and found the size started to increase but the PDI did not change much, suggesting the main reason for the size increase could be attributed to polymer swelling instead of aggregation of nanoparticles. On day 56, 7× PBS exhibited the smallest size and PDI, appearing to be the best formulation. Therefore, we demonstrated that the salt concentration screening method can successfully identify the best salt concentration for making stable and uniform polymer nanoparticles with high docetaxel loading (49.5 wt%).

3.3 | Salt-induced liquid-liquid phase separation

Next, we investigated the salting-out process under different conditions. Using the same ingredients as our screening study, we first investigated mixing a portion of the solvent DMF with different portions (0.2 to 3) of 7× PBS (Figure 3A). To clearly visualize the phase separation, we dissolved a hydrophilic fluorescent dye, fluorescein isothiocyanate-dextran with an average molecular weight of 40,000 Da (FITC-$Dextran_{40k}$), in the PBS. The fluorescent group of FITC-$Dextran_{40k}$, fluorescein, has strong green fluorescence in water but weak fluorescence in DMF due to the different hydrogen bonding abilities of solvents.[28] Therefore, we can easily distinguish the water phase and solvent phase by fluorescence labeling. Strong fluorescence represents the water phase whereas weak fluorescence represents the DMF phase.

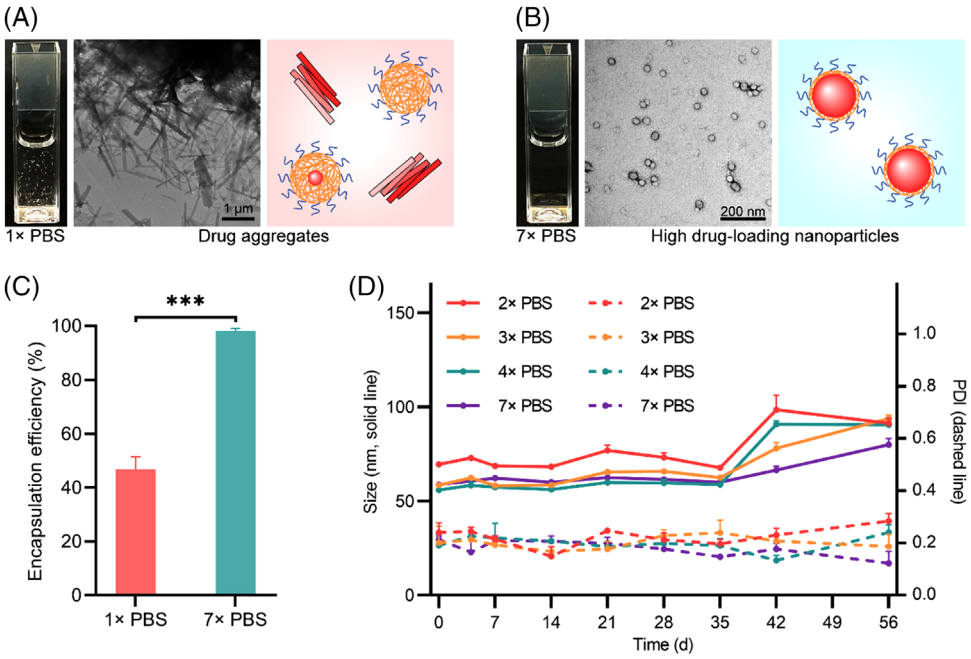

FIGURE 2 The comparison of 50 wt% docetaxel-loaded $PLGA_{10k}$-PEG_{5k} nanoparticles produced using bad and good salt concentrations. The snapshot, TEM image, and schematic for the nanoparticles produced by (A) bad salt concentration (1× PBS) and (B) good salt concentration (7× PBS). The suspension was stirred before taking the snapshot to show the aggregates. (C) Comparison of the encapsulation efficiency for the nanoparticles produced by 1× and 7× PBS. The mean ± s.d. from three independent replicates is shown. ***$p < 0.001$, analyzed by two-tailed Student's t-test. (D) Stability of the nanoparticles produced by four good salt concentrations, 2×, 3×, 4×, and 7× PBS for 56 days at 4°C

First, we examined the effect of volume ratios of DMF to PBS on phase separation. One portion of DMF was mixed with different portions of 7× PBS ranging from a volume ratio of 1:0.2 to 1:3 (Figure 3B). Starting from 1:0.2, microdroplets were observed as the dispersed phase. This water-DMF liquid-liquid phase separation was induced by the salts present in 7× PBS (Table S1), though water and DMF are miscible in all ratios without salts.[29] These microdroplets had strong green fluorescence compared to the dark continuous phase, indicating the droplets were water-rich phase and the continuous phase was the DMF-rich phase (Figure 3C). With the increase of DMF:PBS ratio to 1:1, the droplets continuously grew bigger, indicating a greater phase separation. However, the droplets became smaller at the DMF:PBS ratio of 1:1.5, and finally disappeared at 1:2, showing the phase fusion. During the process of adding 7× PBS, the dispersed phase was always water-rich phase indicated by the fluorescence of $FITC\text{-}Dextran_{40k}$. When the phases fused in the end, the entire solution showed strong fluorescence due to the final water-rich environment.

Then, we investigated the effect of different salt concentrations on phase separation. Keeping the volume ratio of DMF and PBS as 1:1, we tuned the PBS concentrations from 1× to 15× (Figure 3D). The commonly used PBS concentration for nanoprecipitation, 1×, did not yield any phase separation (Figure 3E,F). However, starting from 3× PBS, micro water droplets could be observed as evidenced by the green fluorescence from $FITC\text{-}Dextran_{40k}$. Until the PBS concentration increased to 15×, the size of the micro water droplets kept increasing, suggesting the positive correlation between the salt concentration and the phase separation efficiency.

As demonstrated, the salt-induced liquid-liquid phase separation contributes to the successful formation of high drug-loading nanoparticles. The formation of water-rich microdroplets in high salt conditions separated the water phase from the continuous solvent phase, providing a more solvent-rich hydrophobic continuous environment compared to solutions with no phase separation, thus delaying the precipitation of the dissolved drugs and polymers.

3.4 | Effect of salt concentration on drug and polymer precipitation

To test the hypothesis that the phase separation may delay the precipitation time of drugs or polymers, we further investigated the nanoprecipitation process of dissolved drugs and polymers at different salt concentrations. Derived count rates (DCR), determined by dynamic light scattering (DLS), have been used as an indicator for the mass concentration of dispersed particles in suspensions.[30–32] Here we used the product of a DCR value (kcps) and the corresponding volume (mL) of suspension as the indicator of accumulative nanoprecipitation. The DCR of pure DMF-PBS mixture with no drug was regarded as the blank for subtraction. By adding 1× PBS to DMF containing the drug (5 g/L docetaxel), the accumulative nanoprecipitation increased with PBS/DMF ratio, finally reaching the plateau at the complete precipitation (Figure 4A). Higher salt concentrations (3×, 5×, and 7×) exhibited delayed drug precipitation, e.g., 1× and 7× PBS resulted in complete drug precipitation at PBS/DMF ratios of 1.2 and 1.8, respectively, proving our hypothesis. Similarly, the polymer (5 g/L $PLGA_{10k}$-PEG_{5k}) also showed delayed precipitation with the increase in salt concentration (Figure 4B).

Interestingly, when we attempted to correlate drug and polymer precipitation time with the phase separation-fusion process (Figures 4A,B and 3G), we found that most of the drug and polymer precipitated during the phase fusion stage. For example, in 3× PBS, most drug and polymer

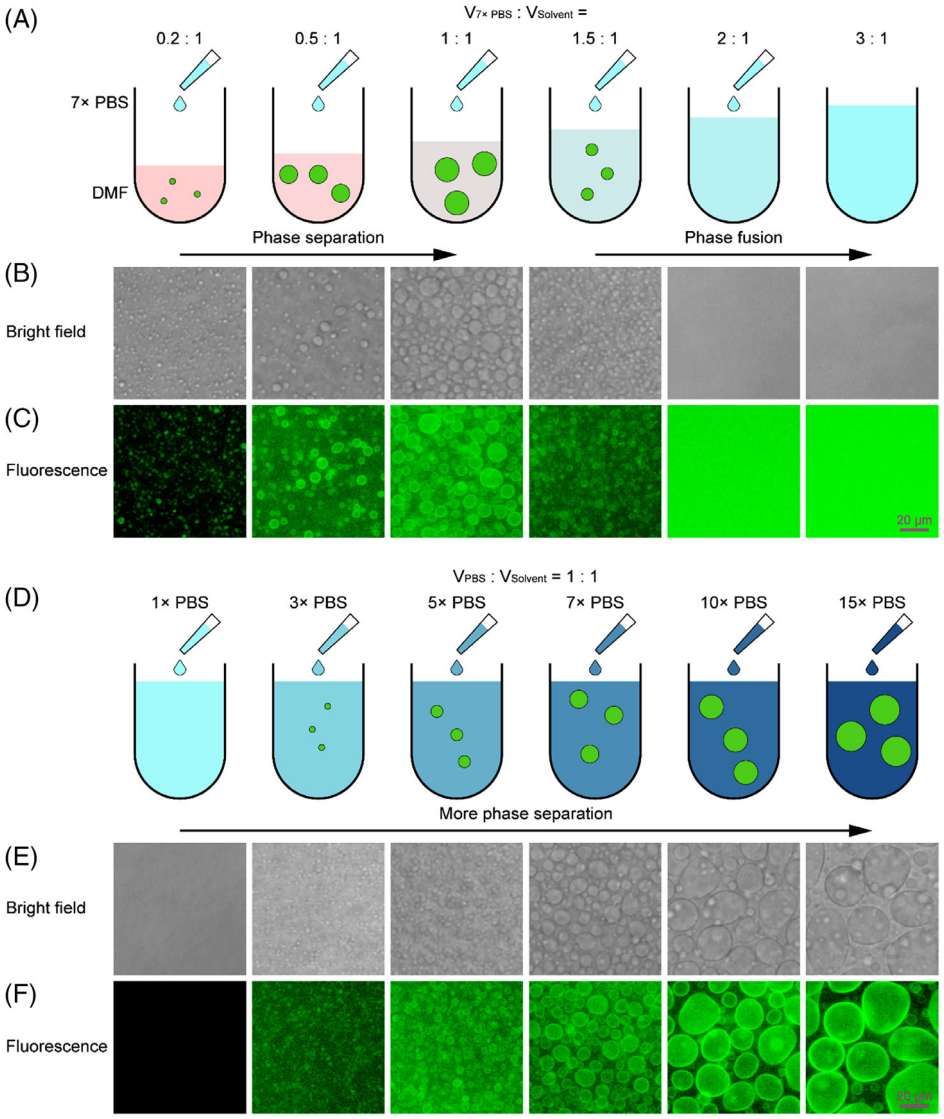

FIGURE 3 Salt-induced liquid-liquid phase separation. (A) Schematic, (B) bright field, and (C) fluorescence images of the mixture comprising of 7× PBS containing FITC-Dextran as a marker and DMF with volume ratios from 0.2:1 to 3:1 ($V_{7\times PBS}$ / V_{DMF}). The (D) schematic, (E) bright field, and (F) fluorescence images of the mixture comprising of DMF and 1×, 3×, 5×, 7×, 10×, and 15× PBS at the volume ratio of 1:1. Scale bars (20 μm) apply to all images in (B,C,E,F)

precipitated at PBS/DMF ratios of 1.0 to 1.4 (Figure 4A,B). 5× and 7× PBS demonstrated similar precipitation timing. This phenomenon demonstrated that the phase separation included by salts could confine the drug in the solvent-rich hydrophobic phase from water-rich droplets. While upon the addition of more PBS solution, the sudden phase fuse leads to a flash co-precipitation thus the formation of nanoparticles with high drug loading.

Furthermore, we also analyzed the distributive nanoprecipitation diagrams of drugs and polymers at different salt concentrations. We used the same drug and polymer concentrations (both at 5 g/L in DMF) to make an initial drug loading of 50 wt%. The overall delayed precipitation trend of both drugs and polymers can be clearly observed (Figure 4C,D). We also analyzed the precipitation diagrams of the drug and the polymer for each salt concentration (Figure 4E). The commonly used condition for making drug-loaded nanoparticles, 1× PBS, demonstrated very different distributive precipitation diagrams, leading to the separate precipitation of the drug and the polymer thus forming large drug aggregates at the 50 wt% initial drug loading using 1× PBS (Figure 2A). In contrast, the distributive precipitation diagrams of the drug and the polymer showed a considerable overlap using 3× PBS, resulting in co-precipitation (Figure 4F). 5× PBS presents separate precipitation again, whereas 7× PBS exhibits the highest degree of overlapping thus the best co-precipitation (Figure 4G,H). This corresponds well with the quality and stability of the various nanoparticles formed in different salt conditions (Figures 1C and 2), suggesting that the best co-precipitation results in the best high drug-loading nanoparticles. Co-precipitation is important for making small high drug-loading nanoparticles and achieving high encapsulation efficiency.[33] Therefore, screening salt concentrations is an efficient way for searching the optimal condition for the co-precipitation of drugs and polymers thus the successful formation of fine nanoparticles with high drug loading.

3.5 | Encapsulation of different drugs

We applied this salt concentration screening method for different drugs and polymers. A wide range of high

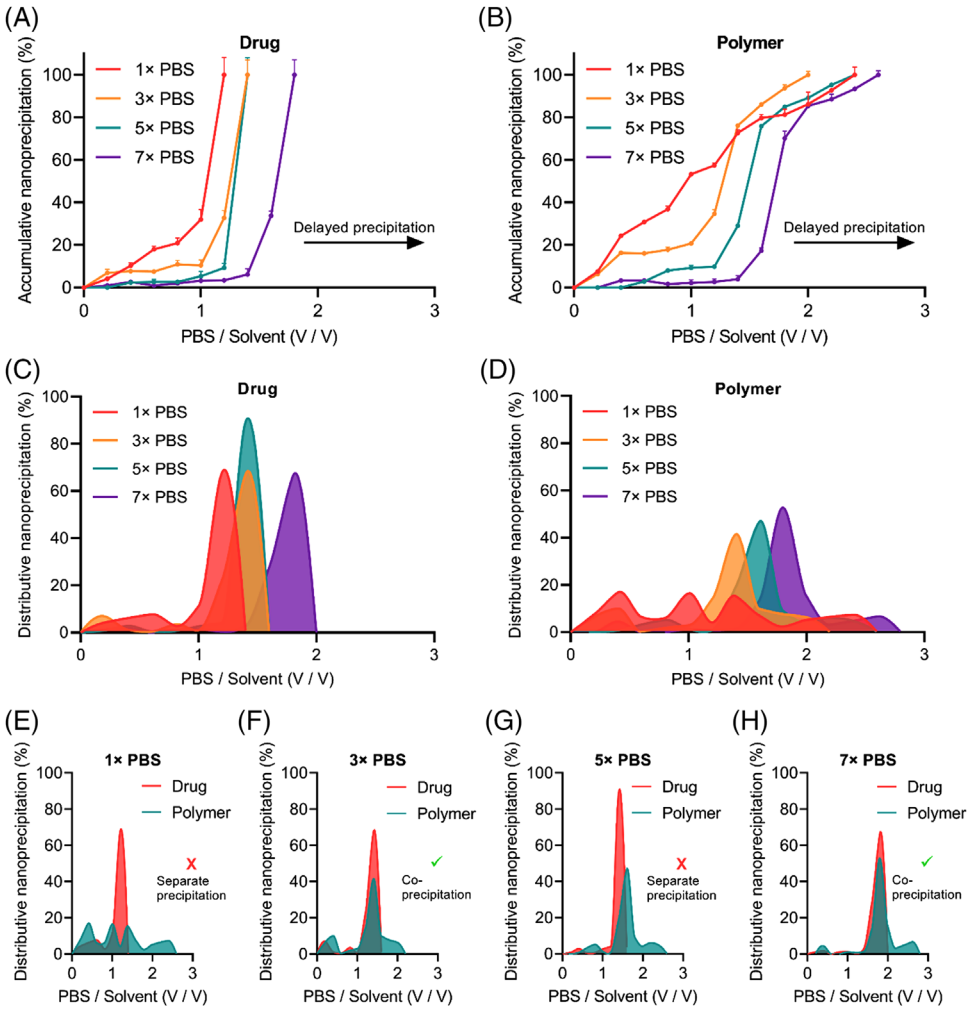

FIGURE 4 The accumulative and distributive drug and polymer precipitation diagrams for antisolvents of 1×, 3×, 5×, and 7× PBS. The accumulative precipitation diagrams of (A) drug (5 g/L docetaxel in DMF) and (B) polymer (5 g/L $PLGA_{10k}$-PEG_{5k} in DMF), and the distributive precipitation diagrams of (C) drug and (D) polymer for the antisolvent of 1×, 3×, 5×, and 7× PBS. The distributive precipitation diagrams of drug and polymer for individual salt concentrations for (E) 1×, (F) 3×, (G) 5×, and (H) 7× PBS

docetaxel-loading nanoparticles can be successfully generated (Figures 5A–C, S2, S3, Tables S5–S9), and the encapsulation efficiencies were all above 90%. Strikingly, an extraordinary drug loading of 66.5 wt% was achieved at 14× PBS (Figure 5C), and the nanoparticles had a hydrodynamic size of 90 nm and PDI of 0.2. Interestingly, we can find that the higher the drug loading is, the more difficult it is to identify the good salt concentration. For instance, only one salt concentration (10× and 14×) was identified for the 60 and 70 wt% drug loadings, respectively, probably due to the very narrow co-precipitation windows of the drug and polymer at higher drug loadings.

In addition to docetaxel, other hydrophobic drugs or dyes including ibuprofen, ketamine, tetramethylindocarbocyanine perchlorate (DiI), and curcumin have also been successfully encapsulated to form nanoparticles with high cargo-loading using the same salt concentration screening method (Figure 5D–F, Tables S4, S10–S13), demonstrating the versatility of this method. In addition to the widely used polymer $PLGA_{10k}$-PEG_{5k}, we also attempted other polymers such as $PLGA_{55k}$-PEG_{5k}, shellac, PLA_{9k}-PEG_{3k}, and PCL_{20k}-PEG_{5k} to encapsulate the model drug docetaxel, and discovered good salt concentrations as well (Figure 5G–J, Tables S14 and S15). It should be noted that some drugs and polymers could co-precipitate at low salt concentrations without the help of phase separation (Figure 5H). But the phase separation-induced nanoprecipitation method is powerful for making high drug-loading nanoparticles by screening a wide range of drugs and polymers that cannot naturally co-precipitate. Moreover, another water-miscible solvent dimethyl sulfoxide (DMSO) could also be used for making 50 wt% docetaxel-loading nanoparticles (Figure 5K and Table S16). In addition, another buffer system using HEPES and NaCl has been explored to form docetaxel-loaded $PLGA_{10k}$-PEG_{5k} nanoparticles with high drug loading (Figure 5L). It should be noted that the good salt conditions were sometimes continuous (Figure 5D,H,K,L) whereas sometimes discontinuous (Figures 1C and 5A,E,F,G,I,J). This mainly depends on whether such salt concentration can induce the co-precipitation of the drug and the polymer (Figure 4E–H). Therefore, the salt concentration screening method is a universal and effective method for producing high drug-loading nanoparticles. It induces liquid-liquid phase separation at high salt concentrations, confining drugs and polymers in the more hydrophobic continuous phase from water droplet phase, thus delaying their precipitation time and facilitating the co-precipitation of drugs and polymers, ultimately

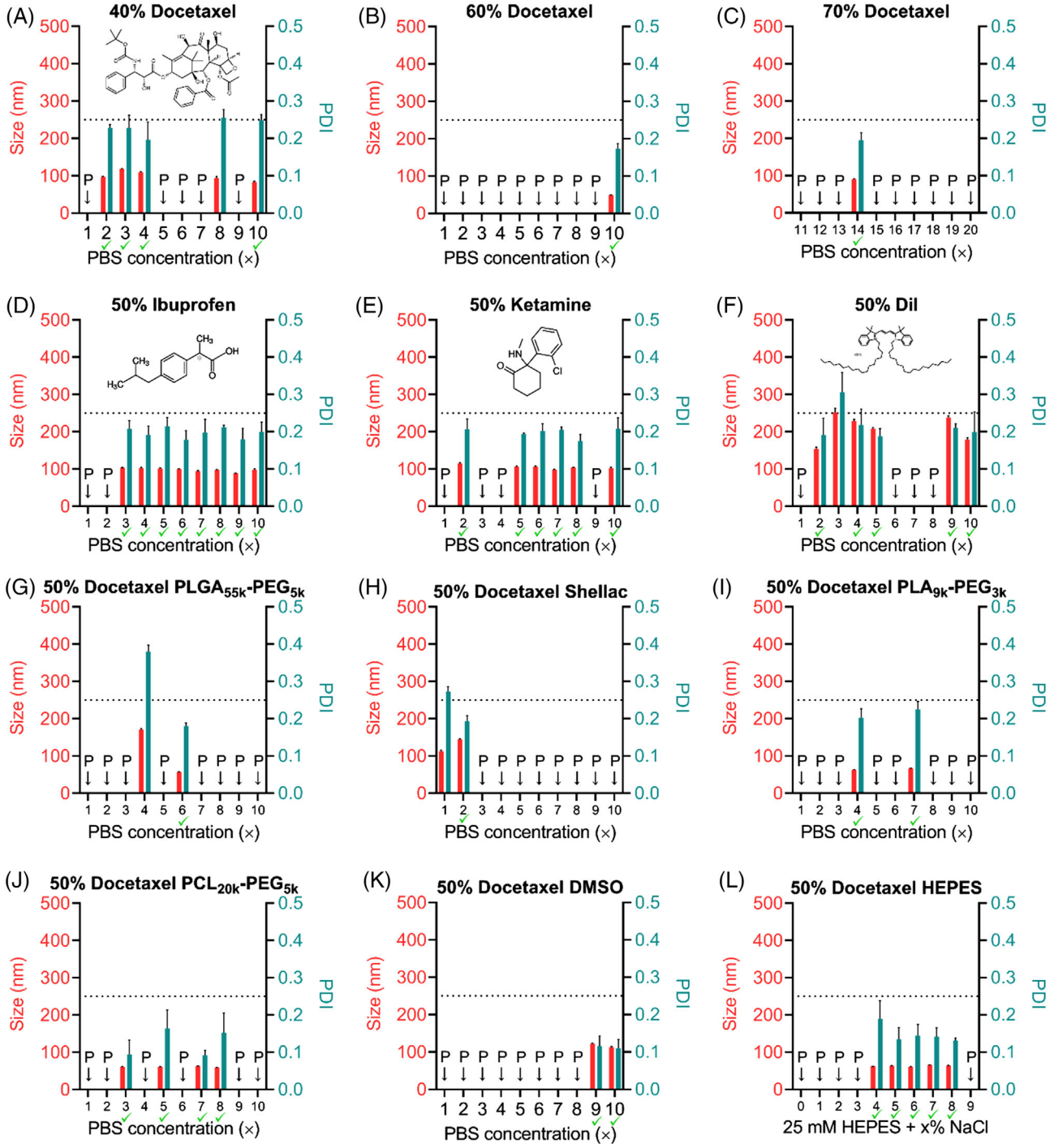

FIGURE 5 The salt-concentration screening method can be applied to different drug loadings, drugs, polymers, and solvents. This method allows the successful screening of good salt concentrations for making (A) 40 wt%, (B) 60 wt%, and (C) 70 wt% docetaxel-loaded $PLGA_{10k}$-PEG_{5k} nanoparticles, and 50 wt% (D) ibuprofen, (E) ketamine, and (F) DiI loaded $PLGA_{10k}$-PEG_{5k} nanoparticles. It also successfully screened the good salt concentrations of 50 wt% docetaxel loaded (G) $PLGA_{55k}$-PEG_{5k}, (H) shellac nanoparticles, (I) PLA_{9k}-PEG_{3k}, (J) PCL_{20k}-PEG_{5k}, and the 50 wt% docetaxel loaded $PLGA_{10k}$-PEG_{5k} using (K) DMSO replacing DMF and (L) HEPES+0-9%NaCl replacing 1–10× PBS. Green ticks indicate good formulations.

the formation of nanoparticles with exceptionally high drug loadings.

4 | CONCLUSIONS

In summary, this paper reports for the first time the salt-concentration screening method for making polymer nanoparticles with tunable drug loadings. Owing to the liquid-liquid phase separation induced by high salt concentrations, water-rich dispersed phase and solvent-rich continuous phase can be formed. This provides a more hydrophobic environment for the drugs and polymers dissolved in the continuous phase, delaying their precipitation time and facilitating their co-precipitation. As a result, one or more good salt concentrations can be identified. The drug-loaded nanoparticles made using the optimal salt concentration can achieve extraordinarily high drug loading (up to 66.5 wt%), high encapsulation efficiency (up to 99.8%), and excellent stability (longer than one month). Moreover, this method is versatile and can be adapted to various hydrophobic drug and dye molecules including docetaxel, ibuprofen, ketamine,

curcumin, and DiI. It is also highly tunable as different drug loadings (19.1–66.5 wt%), polymers ($PLGA_{10k}$-PEG_{5k}, $PLGA_{55k}$-PEG_{5k}, and shellac), and even solvents (DMF and DMSO) can be used. This salt concentration screening method is straightforward, which only needs to screen the antisolvent. It opens a new strategy to fabricate nanoparticles with high drug loading and offers new opportunities for future advances in the field of nanomedicine and drug delivery.

ACKNOWLEDGMENTS

This work was supported by the Australian Research Council (DP200101238) and National Health and Medical Research Council projects of Australia APP2008698. The authors acknowledge Dr. Felicity Han for providing ketamine. The authors acknowledge the facilities, and the scientific and technical assistance, of the Australian Microscopy & Microanalysis Research Facility at the Centre for Microscopy and Microanalysis, The University of Queensland.

CONFLICT OF INTEREST

C.-X.Z., Y.L., and G.Y. are inventors on a patent related to this work (PCT/AU2020/051311) filed by the University of Queensland. All other authors declare no conflict of interest.

ETHICS STATEMENT

There are no ethical issues in this work.

ORCID

Dong Chen https://orcid.org/0000-0002-8904-9307
Chun-Xia Zhao https://orcid.org/0000-0002-3365-3759

REFERENCES

1. S. M. D'Addio, R. K. Prud'homme, *Adv. Drug Deliv. Rev.* **2011**, *63*, 417.
2. X. Yan, J. Bernard, F. Ganachaud, *Adv. Colloid Interface Sci.* **2021**, 102474.
3. W. Li, Q. Chen, T. Baby, S. Jin, Y. Liu, G. Yang, C.-X. Zhao, *Chem. Eng. Sci.* **2021**, *235*, 116468.
4. C. J. M. Rivas, M. Tarhini, W. Badri, K. Miladi, H. Greige-Gerges, Q. A. Nazari, S. A. G. Rodríguez, R. Á. Román, H. Fessi, A. Elaissari, *Int. J. Pharm.* **2017**, *532*, 66.
5. G. Yang, Y. Liu, Y. Hui, D. Chen, D. A. Weitz, C. X. Zhao, *Angew. Chem. Int. Ed.* **2021**.
6. S. Shen, Y. Wu, Y. Liu, D. Wu, *Int. J. Nanomed.* **2017**, *12*, 4085.
7. Y. Liu, G. Yang, S. Jin, L. Xu, C. X. Zhao, *ChemPlusChem* **2020**, *85*, 2143.
8. G. M. Soliman, *Int. J. Pharm.* **2017**, *523*, 15.
9. Y. Liu, G. Yang, S. Jin, R. Zhang, P. Chen, L. Wang, D. Chen, D. A. Weitz, C. X. Zhao, *Angew. Chem. Int. Ed.* **2020**, *59*, 20065.
10. Y. Liu, G. Yang, S. Jin, R. Zhang, P. Chen, L. Wang, D. Chen, D. A. Weitz, C. X. Zhao, *Angew. Chem. Int. Ed.* **2020**, *132*, 20240.
11. Y. Liu, G. Yang, T. Baby, D. Chen, D. A. Weitz, C. X. Zhao, *Angew. Chem. Int. Ed.* **2020**, *132*, 4750.
12. H. Shen, S. Hong, R. K. Prud'homme, Y. Liu, *J. Nanopart. Res.* **2011**, *13*, 4109.
13. E. Lepeltier, C. Bourgaux, P. Couvreur, *Adv. Drug Deliv. Rev.* **2014**, *71*, 86.
14. Y. Liu, G. Yang, Y. Hui, S. Ranaweera, C. X. Zhao, *Small* **2022**, 2106580.
15. S. Gräslund, P. Nordlund, J. Weigelt, B. M. Hallberg, J. Bray, O. Gileadi, S. Knapp, U. Oppermann, C. Arrowsmith, R. Hui, *Nat. Methods* **2008**, *5*, 135.
16. D. Hekmat, *Bioprocess Biosyst. Eng.* **2015**, *38*, 1209.
17. C. Fu, Z. Li, Z. Sun, S. Xie, *Front. Chem. Sci. Eng.* **2021**, *15*, 854.
18. P. Novák, V. Havlíček in *Proteomic Profiling and Analytical Chemistry* (Eds: P. Ciborowski, J. Silberring), Elsevier **2013**, pp. 79–90.
19. H. Ibrahim, C. Bindschaedler, E. Doelker, P. Buri, R. Gurny, *Int. J. Pharm.* **1992**, *87*, 239.
20. E. Allémann, J.-C. Leroux, R. Gurny, E. Doelker, *Pharm. Res.* **1993**, *10*, 1732.
21. A. Salis, M. Monduzzi, *Curr. Opin. Colloid Interface Sci.* **2016**, *23*, 1.
22. P. W. Voorhees, *J. Stat. Phys.* **1985**, *38*, 231.
23. Y. Liu, K. Kathan, W. Saad, R. K. Prud'homme, *Phys. Rev. Lett.* **2007**, *98*, 036102.
24. B. A. Legg, M. Zhu, L. R. Comolli, B. Gilbert, J. F. Banfield, *Environ. Sci. Technol.* **2014**, *48*, 13703.
25. A. M. Vindedahl, J. H. Strehlau, W. A. Arnold, R. L. Penn, *Environ. Sci.: Nano* **2016**, *3*, 494.
26. L. Xu, H.-W. Liang, Y. Yang, S.-H. Yu, *Chem. Rev.* **2018**, *118*, 3209.
27. K. Ulbrich, K. Hola, V. Subr, A. Bakandritsos, J. Tucek, R. Zboril, *Chem. Rev.* **2016**, *116*, 5338.
28. M. M. Martin, *Chem. Phys. Lett.* **1975**, *35*, 105.
29. R. A. Persichetti, N. L. Clair, J. P. Griffith, M. A. Navia, A. L. Margolin, *J. Am. Chem. Soc.* **1995**, *117*, 2732.
30. G. Bastiat, C. O. Pritz, C. Roider, F. Fouchet, E. Lignières, A. Jesacher, R. Glueckert, M. Ritsch-Marte, A. Schrott-Fischer, P. Saulnier, *J. Controlled Release* **2013**, *170*, 334.
31. P. Babakhani, R.-a. Doong, J. Bridge, *Environ. Sci. Technol.* **2018**, *52*, 8419.
32. P. Babakhani, J. Bridge, T. Phenrat, F. Fagerlund, R.-a. Doong, K. R. Whittle, *Colloids Surf. A* **2019**, *582*, 123862.
33. W. S. Saad, R. K. Prud'homme, *Nano Today* **2016**, *11*, 212.

SUPPORTING INFORMATION

Additional supporting information can be found online in the Supporting Information section at the end of this article.

How to cite this article: G. Yang, Y. Liu, S. Jin, Y. Hui, X. Wang, L. Xu, D. Chen, D. Weitz, C.-X. Zhao, *Aggregate* **2023**, e314. https://doi.org/10.1002/agt2.314